Photosynthetic reaction center as a quantum heat engine

Konstantin E. Dorfman[a,b,c,1], Dmitri V. Voronine[a,b,1], Shaul Mukamel[c], and Marlan O. Scully[a,b,d]

[a]Texas A&M University, College Station, TX 77843-4242; [b]Princeton University, Princeton, NJ 08544; [c]University of California, Irvine, CA 92697-2025; and [d]Baylor University, Waco, TX 76798

Edited by Graham R. Fleming, University of California, Berkeley, CA, and approved November 15, 2012 (received for review July 26, 2012)

Two seemingly unrelated effects attributed to quantum coherence have been reported recently in natural and artificial light-harvesting systems. First, an enhanced solar cell efficiency was predicted and second, population oscillations were measured in photosynthetic antennae excited by sequences of coherent ultrashort laser pulses. Because both systems operate as quantum heat engines (QHEs) that convert the solar photon energy to useful work (electric currents or chemical energy, respectively), the question arises whether coherence could also enhance the photosynthetic yield. Here, we show that both effects arise from the same population–coherence coupling term which is induced by noise, does not require coherent light, and will therefore work for incoherent excitation under natural conditions of solar excitation. Charge separation in light-harvesting complexes occurs in a pair of tightly coupled chlorophylls (the special pair) at the heart of photosynthetic reaction centers of both plants and bacteria. We show the analogy between the energy level schemes of the special pair and of the laser/photocell QHEs, and that both population oscillations and enhanced yield have a common origin and are expected to coexist for typical parameters. We predict an enhanced yield of 27% in a QHE motivated by the reaction center. This suggests nature-mimicking architectures for artificial solar energy devices.

photosynthesis | quantum biology | population oscillations | quantum coherence

According to the laws of quantum thermodynamics, quantum heat engines (QHEs) convert hot thermal radiation into low-entropy useful work (1, 2). The ultimate efficiency of such QHEs is usually governed by a detailed balance between absorption and emission of the hot pump radiation (3). The laser is an example of a QHE, which can use incoherent pump (heat) radiation to produce highly coherent (low-entropy) light (Fig. 1 *A* and *B*). Moreover, it was demonstrated both theoretically and experimentally that noise-induced quantum coherence (4) can break detailed balance and yield lasers without population inversion (5) and/or with enhanced efficiency (Fig. 1*C*).

Recently it has been shown that quantum coherence can, in principle, enhance the efficiency of a solar cell or a photodetector (6–10). This photocell QHE (Fig. 1*D*) can be described by the same model as the laser QHE (Fig. 1*E*) and obeys similar detailed balance physics. To use the broad solar spectrum and eliminate phonon loss, we separate solar flux into narrow frequency intervals and direct it onto a cell array where each of the cells has been prepared to have its band gap equal to that photon energy (7). In particular, Shockley and Queisser (11) invoked detailed balance to show that the open-circuit voltage of a photocell is related to the energy input of a "hot" monochromatic thermal light by the Carnot factor. However, just as in the case of the laser, we can, in principle, break detailed balance by inducing coherence (Fig. 1*F*), which can enhance the photocell efficiency (9, 10).

Other recent papers investigated the common ground between photovoltaics and photosynthetic light harvesting (12, 13). Various models addressed the high efficiency of energy transfer in photosynthetic antennae (14–19) and the mechanisms of charge separation in reaction centers (12, 20–22). Furthermore, quantum coherence effects, e.g., photon echo, have been observed in a series of interesting photosynthesis experiments (23–30). Oscillations of exciton population signals in the 2D photon echo (rephasing) spectra have been predicted (31) and directly observed (32) as evidence of quantum transport. However, because multidimensional spectroscopy uses coherent laser radiation as a source of quantum coherence, the quantum effects that might be observed under natural conditions of excitation by incoherent solar light are still an open issue.

Coherent versus incoherent energy transfer has long been studied in molecular crystals and aggregates (33–35). It is well established that the interplay between exciton coupling and energetic disorder controls the extent of exciton delocalization, which in turn determines the nature of transport (36). Coherent effects become more prominent as the excitons become more delocalized. Recent femtosecond experiments in photosynthetic complexes have revived the interest in the same issues. Oscillatory temporal features in 2D spectra have been initially attributed to electronic coherence but growing evidence indicates that this could be due as well to strongly coupled vibronic motions (37–40). The simplest approach to energy transfer is based on the Redfield equations that treat the system/bath coupling perturbatively to second order. They are invariant to the exciton basis and can be applied to localized and delocalized excitons alike (41). The Förster theory of energy transfer and the Marcus theory of charge transfer assume localized states. Like the Redfield equations they treat off-diagonal couplings perturbatively but include diagonal bath fluctuations (polaron effects) to high order. Both theories can be derived in a very transparent way by using a unified formalism of bath fluctuations based on the cumulant expansion (20, 42).

We apply the physics of the laser and photocell described above to investigate these effects in a QHE inspired by photosynthetic complexes. In the model of Fig. 2*B*, the broad solar spectrum can be used by various photosynthetic antennae complexes which transfer energy to the reaction center. The antennae absorb broadband light in the visible range and relax to the bottom of the excited band due to rapid thermalization. They transfer narrowband excitation to the reaction center (13). We adopt the level schemes of Fig. 2 *B* and *E* to describe collective excitations in molecular aggregates and show that quantum coherence may increase the efficiency of photosynthesis. We demonstrate that the photosynthetic reaction center may be viewed as a biological quantum heat engine (BQHE) that transforms high-energy thermal photon radiation into low-entropy electron flux (Fig. 2*A*, adapted from ref. 31) and estimate the role of noise-induced quantum

Author contributions: K.E.D., D.V.V., S.M., and M.O.S. designed research; K.E.D. and D.V.V. performed research; and K.E.D., D.V.V., S.M., and M.O.S. wrote the paper.

The authors declare no conflict of interest.

This article is a PNAS Direct Submission.

[1]To whom correspondence may be addressed. E-mail: dmitri.voronine@gmail.com or kdorfman@uci.edu.

This article contains supporting information online at www.pnas.org/lookup/suppl/doi:10.1073/pnas.1212666110/-/DCSupplemental.

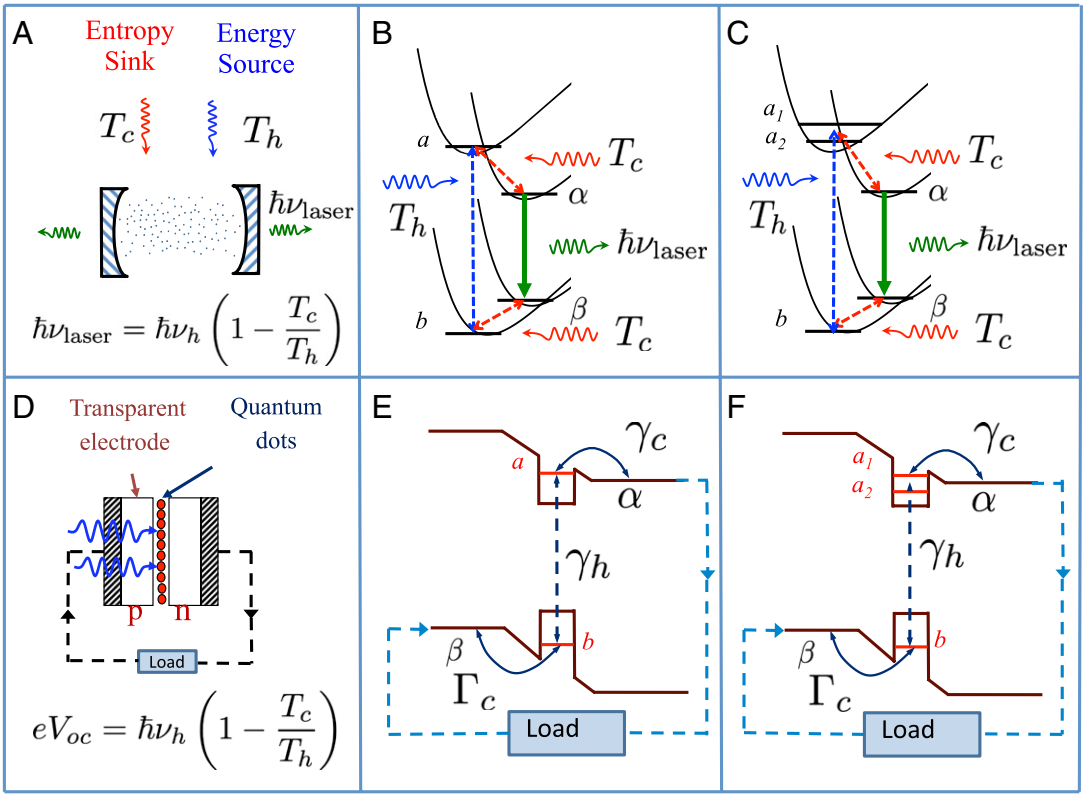

Fig. 1. Schemes of a laser QHE (*A*) and a photocell QHE consisting of quantum dots sandwiched between *p*- and *n*-doped semiconductors (*D*). These QHEs are pumped by hot photons at temperature T_h (energy source, blue) and by cold photons or phonons at temperature T_c (entropy sink, red) and operate with quantum efficiency governed by the Carnot relation. Schemes of four-level molecules inside the laser cavity (*B*) and electronic states of the quantum dot photocell (*E*). Optical transitions $b \leftrightarrow a$ and $a \leftrightarrow \alpha$ ($b \leftrightarrow \beta$) are driven by "hot" photons and ambient "cold" phonons, respectively. *C* and *F* are the same as *B* and *E*, respectively, with the upper level *a* replaced by two levels a_1 and a_2. The QHE power of the five-level system in *C* and *F* can be doubled compared with the four-level system in *B* and *E* when there is coherence between these levels.

coherence on the efficiency of charge separation. This insight leads to a unified picture of two seemingly unrelated quantum coherence effects: oscillation of populations and enhanced electric current in the BQHE. The ultimate efficiency is bound by the Carnot limit, consistent with the second law of thermodynamics.

We describe the photoinduced charge separation between the donor D and the acceptor A molecules interacting with thermal light (Fig. 2*B*) using the four-level QHE scheme shown in Fig. 2*E*. State b corresponds to the lowest energy configuration where both molecules are in the ground states. State a describes the configuration where donor D is excited (both the excited electron and the hole are in donor D); α is a charge-separated state with the electron in acceptor A and the hole in donor D. Finally, β is the ionized state where the electron is transferred to a "sink" and the system is positively charged. After absorption of a solar photon, the excited electron is promoted from b to a and is then transferred to α with the excess energy radiated as a phonon. Furthermore, the electron released from state α results in a current from α to β, which we model by a relaxation rate Γ, such that the current $j = e\Gamma\rho_{\alpha\alpha}$ is governed by the population of α. To complete the cycle, we assume that another population transfer takes place which brings the electron back to the ground state b of donor D with emission of a phonon with excess energy.

Quantum coherence can significantly affect the efficiency of this process. Fig. 2*C* shows two closely spaced identical donor molecules D_1 and D_2 that represent a special pair of chlorophylls at the heart of the reaction center complex where the primary charge separation takes place (22). In photosynthesis, the sunlight absorbed by antennae complexes is consequently transferred to the special pair. In our setup, we exclude the antenna and assume that the pair absorbs sunlight cooperatively via the exciton states a_1 and a_2 which are separated by the Davydov splitting (33). In bacterial systems the splitting is on the order of 450–800 wavenumbers (43), whereas in the Photosystem II reaction center, the special pair coupling is weaker (160–200 cm^{-1}) (21). The remaining states are similar to those of Fig. 2*E*. As was shown in refs. 9 and 10, the model in Fig. 2*F* can exhibit noise-induced quantum coherence due to Fano interference. This effect originates from the coupling of two levels to the same continuum (4). The initial excitation of states a_1 and a_2 can be transferred to the acceptor molecule in state α by emission of a phonon and can produce useful work by contributing to the electric current and returning to b via β. On the other hand, the system can return to b via stimulated or spontaneous emission. Fano interference can minimize the latter process by inducing coherence between a_1 and a_2 (*SI Text*). Then the net absorption is enhanced and the electron flux is increased.

Identifying the primary electron donors and dominating charge-separation pathways has been a question of recent extensive research and debate. At the moment, there is much evidence that two main pathways make significant contributions under ambient conditions and the lowest energy states depend on disorder (44–47). Whereas in bacterial reaction centers the primary charge separation takes place at the special pair (as used in this work), the reaction centers of Photosystem II also use an additional pathway which starts at the accessory chlorophyll of the *D*1 branch (48, 49). In this work we discuss only the first pathway, which is present in both types of reaction centers and plays an important role in optimizing the electron transfer efficiency. Using design principles inspired by

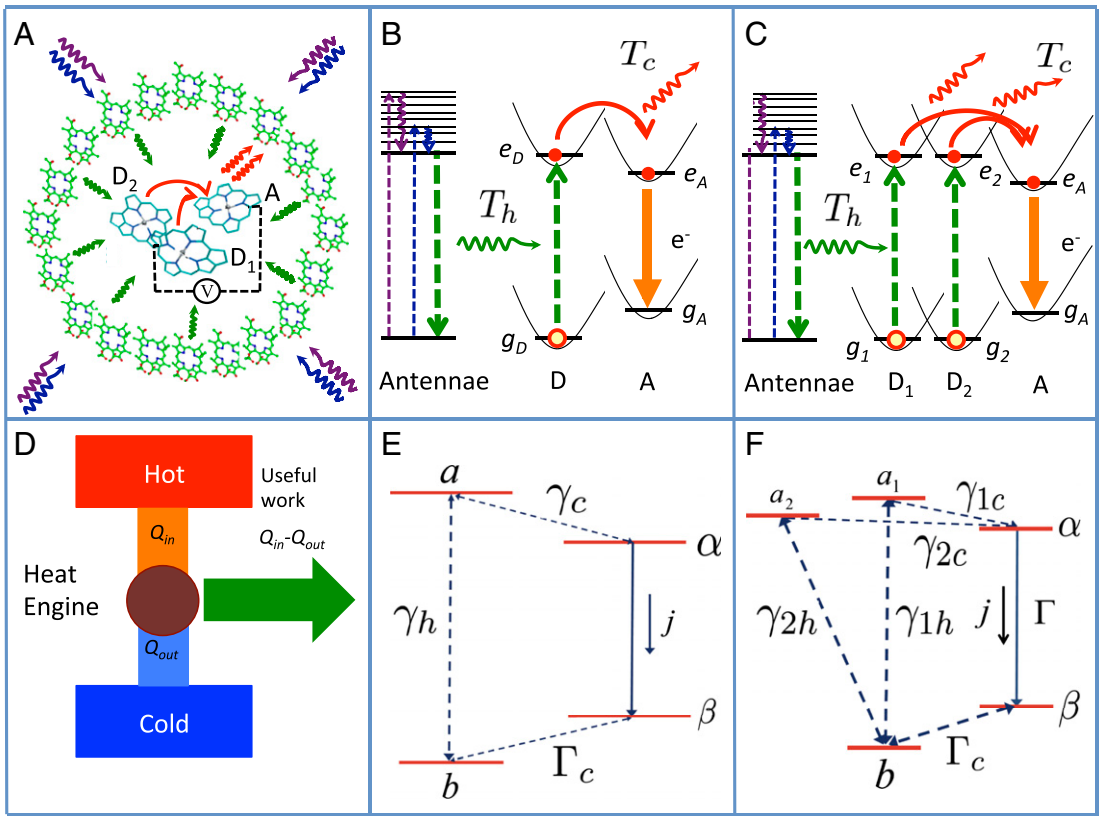

Fig. 2. Schemes of a BQHE based on the photosynthetic reaction center (*A*) and a generic heat engine (*D*). Scheme of charge separation between a donor *D* and an acceptor *A* molecule (*B*). The broad solar spectrum is absorbed by the antennae complexes (arranged in a circle in *A*) which undergo rapid thermalization due to phonon scattering and reach the bottom of the electronic band. Thus, the narrowband excitation is transferred to the reaction center represented by donor and acceptor molecules. *E* represents the generic four-level QHE scheme. *C* and *F* are the same as *B* and *E*, respectively, except that the upper level *a* is replaced by two levels a_1 and a_2 separated by Davydov splitting. The power delivered by the QHE of *C* and *F* can be doubled compared with *B* and *E* if there is coherence between levels a_1 and a_2.

nature, we propose a scheme to design artificial light-harvesting molecular complexes with increased electron transfer efficiency.

The effects of noise-induced coherence can be illustrated by the following equation for the population of state a_1 (50):

$$\dot{\rho}_{11} = -\gamma_{1c}\left[(1+\overline{n}_{1c})\rho_{11} - \overline{n}_{1c}\rho_{\alpha\alpha}\right] - \gamma_{1h}\left[(1+\overline{n}_{1h})\rho_{11} - \overline{n}_{1h}\rho_{bb}\right] - \left[\gamma_{12c}(\overline{n}_{2c}+1) + \gamma_{12h}(\overline{n}_{2h}+1)\right](\rho_{21}+\rho_{12}), \quad [1]$$

where the ρ_{ii} are the populations of levels i, and $\overline{n}_h(\overline{n}_c)$ are the average number of hot solar photons (cold ambient phonons); $\gamma_{1c}(\gamma_{1h})$ are the decay rates from the upper level to levels α and b, respectively; and $\gamma_{12h}(\gamma_{12c})$ are cross-couplings that describe the effect of interference.* The complete set of equations of motion which describe the evolution of all density matrix elements is given in *SI Text*. To obtain a clear physical insight and a qualitative estimate, we consider a simplified model and neglect memory effects (Markov approximation) under the condition of weak system–bath coupling. Future extension to the non-Markovian regime will be necessary to provide a more precise, quantitative calculation of the predicted effects. Recent work has suggested that protein environment plays an important role in photosynthesis (51). The complicated dynamics of strongly coupled protein bath goes beyond the scope of our paper.

*Maximum coherence $\gamma_{12c} = \sqrt{\gamma_{1c}\gamma_{2c}}$ and $\gamma_{12h} = \sqrt{\gamma_{1h}\gamma_{2h}}$; no coherence $\gamma_{12c} = \gamma_{12h} = 0$.

We construct the model in Fig. 2*F* using elements of the reaction center (*SI Text*). Charge separation in a reaction center can be considered as work done by a system similarly to a photovoltaic cell or more generally a QHE powered by thermal radiation of the sun (10). Assuming that α and β are connected by a "load," we introduce the concept of effective voltage V as a drop of the electrostatic potential across the load, which, according to Fermi–Dirac statistics, yields $eV = E_\alpha - E_\beta + k_B T_\alpha \log(\rho_{\alpha\alpha}/\rho_{\beta\beta})$, where E_i is the energy of the state i and e is the electric charge. We apply

Table 1. Summary of the three parameter regimes

	I (Overdamped)	II (Underdamped)	III (Intermediate)
$E_1 - E_2$, cm^{-1}	120	600	720
$E_1 - E_b$, cm^{-1}	14,856	14,856	14,856
$E_1 - E_c$, cm^{-1}	1,611	1,611	1,611
$E_v - E_b$, cm^{-1}	1,611	1,611	1,611
T_s, K	6,000	6,000	6,000
T_a, K	300	300	300
γ_{1h}, cm^{-1}	0.005	0.005	0.005
γ_{2h}, cm^{-1}	0.0016	0.005	0.005
γ_{1c}, cm^{-1}	140	35	280
γ_{2c}, cm^{-1}	18	35	280
Γ_c, cm^{-1}	200	50	300
$1/\tau_2$, cm^{-1}	41	41	41
n_{1h}	60,000	10,000	90,000
n_{2h}	10,000	20,000	10,000

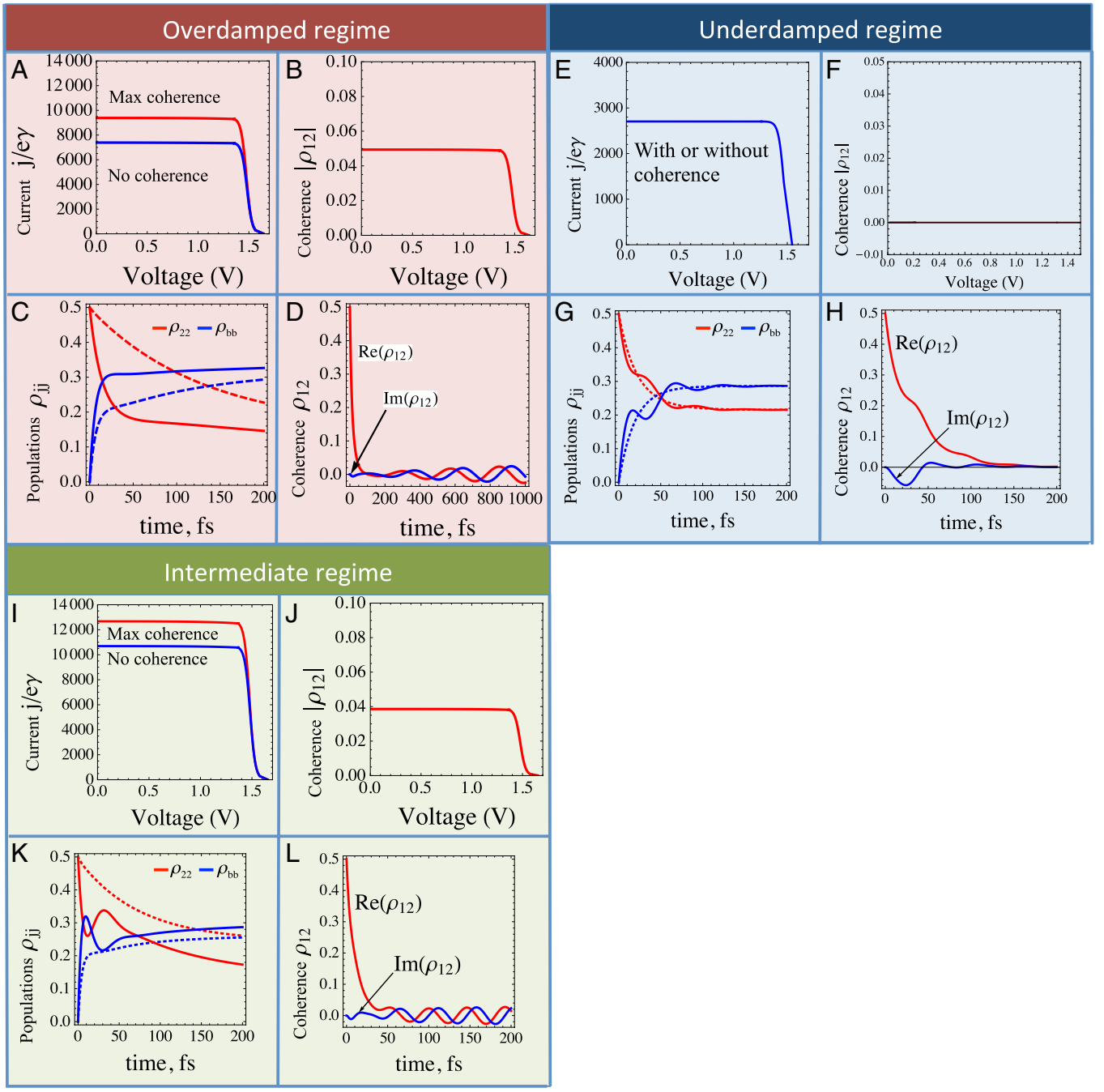

Fig. 3. Steady-state characteristics and excited-state dynamics of a BQHE model of a photosynthetic reaction center in Fig. 2*F*. Three regimes are shown: overdamped (*A–D*); underdamped (*E–H*), and intermediate (*I–L*). Quantum coherence can enhance the electric current by up to 27% in the overdamped and 18% in the intermediate regimes compared with the same five-level system without coherence, whereas no current enhancement is achieved in the underdamped regime. Nonzero steady-state coherence is obtained in *B* and *J*. Populations reveal oscillations in the presence of coherence in *G* and *K* (solid lines), whereas no oscillations are present without coherence (dashed lines). Long-lived coherence is obtained in the overdamped (*D*) and intermediate (*L*) regimes. Parameters corresponding to different regimes are summarized in Table 1 (*Methods*).

this to the steady-state regime and calculate the populations $\rho_{\alpha\alpha}$ and $\rho_{\beta\beta}$ at sufficiently long times. For the operation near the open circuit (weak illumination, no current) the power acquired from the sun is $P_S = j \cdot (E_a - E_b)/e$, whereas the power that can be extracted from the reaction center is $P = j \cdot V_{oc}$. Therefore, the efficiency of such a heat engine $\eta = P/P_S = 1 - T_a/T_S$ is given by the Carnot relation.

Noise-induced coherence is most pronounced if the two interfering levels overlap, i.e., the level spacing is small compared with the inverse lifetimes of a_1 and a_2. In this case, the populations relax exponentially to the steady state. In the opposite limit, quantum coherence manifests itself as oscillations of populations of eigenstates (8, 31). These two limits can be understood by using a simple analogy with the overdamped and underdamped regimes of a harmonic oscillator. Thus, one can associate the enhancement of the steady-state yield with the overdamped regime and population oscillations with the underdamped regime. It is remarkable that both effects are caused by the same mechanism of noise-

induced coherence but realized for different parameters. The summary of parameters used in our simulations is listed in Table 1 of *Methods*. We focus on the Photosystem II reaction center and perform specific simulations using well-known parameters from recent literature (20, 21, 31). We also simulate artificial systems with a broad range of parameters to demonstrate related coherence effects.

We next calculate steady-state current–voltage characteristics for our BQHE model (Fig. 2*F*) in the overdamped regime by increasing the rate Γ from zero (open circuit) to the short-circuit condition (no electrostatic potential across the load). Fig. 3 *A* and *B* depict the normalized electric current and the steady-state coherence ρ_{12} (absolute value), respectively, as a function of the voltage. The red line corresponds to the maximum coherence, whereas the blue line is obtained with no coherence. In this example, noise-induced coherence increases the peak power by about 27% compared with the same five-level system without coherence. The dynamics of populations and coherence ρ_{12} shown in Fig. 3 *C* and *D*, respectively, demonstrate that in this regime there are no population oscillations, whereas coherence oscillates and reaches a steady state.

Fig. 3 *G* and *H* show the population and coherence dynamics, respectively, in the underdamped regime. The oscillatory behavior of populations and coherence is clearly observed on a time scale of $\sim$ 130 fs. This corresponds to the decoherence time after which populations reach the steady-state values as expected for a closed system with a conserved probability. In the absence of coherence, populations evolve exponentially and reach the steady state at nearly the same time as in the presence of coherence. In the underdamped oscillator regime, there is no steady-state coherence (Fig. 3 *E* and *F*) and thus there is no enhancement of the steady-state electric current.

Finally, we investigate the intermediate damping regime where both population oscillations and an enhanced current yield can coexist. Fig. 3 *I* and *J* show the steady-state current–voltage characteristics and coherence as a function of the voltage drop across the acceptor load, respectively. Even for moderate coherence ($\rho_{12} \sim 0.04$), there is an enhancement of 18% in the yield. On the other hand the dynamics of populations and coherence shown in Fig. 3 *K* and *L*, respectively, reveals large-amplitude oscillations on a time scale of $\sim$ 130 fs. Small-amplitude long-lived (steady-state) oscillations of coherences are also present in this regime.

In summary, we describe QHEs inspired by photosynthesis that operate under the natural conditions of incoherent excitation by sunlight using the formalism developed earlier for the laser and photocell engines. This establishes a connection between two previously unrelated effects attributed to quantum coherence: population oscillations in photosynthetic complexes and enhanced photocurrent yield in QHEs. We investigate parameter regimes where large electric current yield enhancement and/or population oscillations are observed and identify noise-induced quantum coherence as the common origin of these effects. In contrast with studies where coherence was generated by laser radiation, this noise-induced coherence requires no external source. Our simulations show that the coherence builds up on a time scale of a few femtoseconds and reaches a steady state in a few nanoseconds. Zero current (open circuit) results in zero coherence whereas steady-state coherence can lead to current enhancement. We find that the structure of the special pair in photosynthetic reaction centers is suitable to use these quantum effects and increase the efficiency of charge separation. Similar noise-induced coherence effects have been experimentally demonstrated in semiconductor quantum wells (52, 53). Our study suggests that these experiments may be extended to photosynthetic complexes and hold promise for improving the design and boosting the efficiencies of light-harvesting devices. A broad range of parameter regimes provides flexibility in designs and materials.

Methods

We use a quantum master equation approach similar to earlier photocell work (*SI Text*) to derive the evolution of the density matrix and obtain steady-state characteristics such as the quantum yield and the electric current. For the simulations shown in Fig. 3 we use the parameters listed in Table 1. Here, $E_1 - E_b$ and $E_1 - E_c$ ($E_v - E_b$) are the transition energies for photons and phonons, respectively; $1/\tau_2$ is the decoherence rate. We assume that the system is irradiated by a concentrated solar radiation with an average number of photons n_{1h} and n_{2h} at energies $E_1 - E_b$ and $E_2 - E_b$, respectively. Due to the large phonon energy (1,611 cm^{-1}) that results in small occupation numbers, we neglect stimulated processes associated with phonons at room temperature. n_{1c} and n_{2c} were set to zero.

ACKNOWLEDGMENTS. K.E.D., D.V.V., and M.O.S. acknowledge the support by National Science Foundation (NSF) Grants PHY-1241032 (INSPIRE CREATIV) and EEC-0540832 (MIRTHE ERC), the Office of Naval Research, and Robert A. Welch Foundation Award A-1261. S.M. acknowledges support from NSF Grant CHE-1058791, Defense Advanced Research Planning Agency BAA-10-40 QuBE, and the Chemical Sciences, Geosciences and Biosciences Division, Office of Basic Energy Sciences, Office of Science, US Department of Energy.

1. Scovil HED, Schulz-DuBois EO (1959) Three-level masers as heat engines. *Phys Rev Lett* 2(6):262–263.
2. Scully MO, Zubairy MS, Agarwal GS, Walther H (2003) Extracting work from a single heat bath via vanishing quantum coherence. *Science* 299(5608):862–864.
3. Einstein A (1917) Zur Quantentheorie der Strahlung. *Phys Z* 18:121–128.
4. Harris SE (1989) Lasers without inversion: Interference of lifetime-broadened resonances. *Phys Rev Lett* 62(9):1033–1036.
5. Scully MO, Zubairy MS (1997) *Quantum Optics* (Cambridge Univ Press, Cambridge, England).
6. Kozlov VV, Rostovtsev Y, Scully MO (2006) Inducing quantum coherence via decays and incoherent pumping with application to population trapping, lasing without inversion, and quenching of spontaneous emission. *Phys Rev A* 74(6):063829.
7. Scully MO (2010) Quantum photocell: Using quantum coherence to reduce radiative recombination and increase efficiency. *Phys Rev Lett* 104(20):207701.
8. Dorfman KE, Jha PK, Das S (2011) Quantum-interference-controlled resonance profiles from lasing without inversion to photodetection. *Phys Rev A* 84(5):053803.
9. Scully MO, Chapin KR, Dorfman KE, Kim MB, Svidzinsky AA (2011) Quantum heat engine power can be increased by noise-induced coherence. *Proc Natl Acad Sci USA* 108(37):15097–15100.
10. Svidzinsky AA, Dorfman KE, Scully MO (2011) Enhancing photovoltaic power by Fano-induced coherence. *Phys Rev A* 84(5):053818.
11. Shockley W, Queisser HJ (1961) Detailed balance limit of efficiency of p-n junction solar cells. *J Appl Phys* 32(3):510–519.
12. Fingerhut BP, Zinth W, de Vivie-Riedle R (2010) The detailed balance limit of photochemical energy conversion. *Phys Chem Chem Phys* 12(2):422–432.
13. Blankenship RE, et al. (2011) Comparing photosynthetic and photovoltaic efficiencies and recognizing the potential for improvement. *Science* 332(6031):805–809.
14. Caruso F, Chin AW, Datta A, Huelga SF, Plenio MB (2009) Highly efficient energy excitation transfer in light-harvesting complexes: The fundamental role of noise-assisted transport. *J Chem Phys* 131(10):105106.
15. Rebentrost P, Mohseni M, Kassal I, Lloyd S, Aspuru-Guzik A (2009) Environment-assisted quantum transport. *New J Phys* 11:033003.
16. Scholes GD (2010) Quantum-coherent electronic energy transfer: Did nature think of it first? *J. Phys. Chem. Lett.* 1(1):2–8.
17. Ishizaki A, Fleming GR (2009) Theoretical examination of quantum coherence in a photosynthetic system at physiological temperature. *Proc Natl Acad Sci USA* 106(41):17255–17260.
18. Lloyd S, Mohseni M (2010) Symmetry-enhanced supertransfer of delocalized quantum states. *New J Phys* 12:075020.
19. Strümpfer J, Sener M, Schulten K (2012) How quantum coherence assists photosynthetic light-harvesting. *J Phys Chem Lett* 3(4):536–542.
20. Abramavicius D, Mukamel S (2010) Energy-transfer and charge-separation pathways in the reaction center of photosystem II revealed by coherent two-dimensional optical spectroscopy. *J Chem Phys* 133(18):184501.
21. Madjet ME, Abdurahman A, Renger T (2006) Intermolecular coulomb couplings from ab initio electrostatic potentials: Application to optical transitions of strongly coupled pigments in photosynthetic antennae and reaction centers. *J Phys Chem B* 110(34):17268–17281.
22. Deisenhofer J, Epp O, Miki K, Huber R, Michel H (1985) Structure of the protein subunits in the photosynthetic reaction centre of Rhodopseudomonas viridis at 3Å resolution. *Nature* 318(6047):618–624.
23. Engel GS, et al. (2007) Evidence for wavelike energy transfer through quantum coherence in photosynthetic systems. *Nature* 446(7137):782–786.
24. Collini E, et al. (2010) Coherently wired light-harvesting in photosynthetic marine algae at ambient temperature. *Nature* 463(7281):644–647.

25. Panitchayangkoon G, et al. (2010) Long-lived quantum coherence in photosynthetic complexes at physiological temperature. *Proc Natl Acad Sci USA* 107(29): 12766–12770.
26. Brixner T, et al. (2005) Two-dimensional spectroscopy of electronic couplings in photosynthesis. *Nature* 434(7033):625–628.
27. Abramavicius D, Palmieri B, Voronine DV, Sanda F, Mukamel S (2009) Coherent multidimensional optical spectroscopy of excitons in molecular aggregates; quasiparticle versus supermolecule perspectives. *Chem Rev* 109(6):2350–2408.
28. Harel E, Engel GS (2012) Quantum coherence spectroscopy reveals complex dynamics in bacterial light-harvesting complex 2 (LH2). *Proc Natl Acad Sci USA* 109(3):706–711.
29. Schlau-Cohen GS, et al. (2012) Elucidation of the timescales and origins of quantum electronic coherence in LHCII. *Nat Chem* 4(5):389–395.
30. Scholes GD, Fleming GR, Olaya-Castro A, van Grondelle R (2011) Lessons from nature about solar light harvesting. *Nat Chem* 3(10):763–774.
31. Abramavicius D, Mukamel S (2010) Quantum oscillatory exciton migration in photosynthetic reaction centers. *J Chem Phys* 133(6):064510.
32. Panitchayangkoon G, et al. (2011) Direct evidence of quantum transport in photosynthetic light-harvesting complexes. *Proc Natl Acad Sci USA* 108(52):20908–20912.
33. Davydov AS (1962) *Theory of Molecular Excitons* (McGraw-Hill, New York).
34. Kenkre VM, Reineker P (1982) *Exciton Dynamics in Molecular Crystals and Aggregates* (Springer, Berlin).
35. Haken H, Strobl G (1967) Exact treatment of coherent and incoherent triplet exciton migration. *The Triplet State*, ed Zahlan AB (Cambridge Univ Press, Cambridge), p 311.
36. Mukamel S (2010) Communications: Signatures of quasiparticle entanglement in multidimensional nonlinear optical spectroscopy of aggregates. *J Chem Phys* 132(24): 241105.
37. Nalbach P, Braun D, Thorwart M (2011) Exciton transfer dynamics and quantumness of energy transfer in the Fenna-Matthews-Olson complex. *Phys Rev E Stat Nonlin Soft Matter Phys* 84(4 Pt 1):041926.
38. Christensson N, Kauffmann HF, Pullerits T, Mančal T (2012) Origin of long-lived coherences in light-harvesting complexes. *J Phys Chem B* 116(25):7449–7454.
39. Chin AW, Huelga SF, Plenio MB (2012) Coherence and decoherence in biological systems: Principles of noise-assisted transport and the origin of long-lived coherences. *Philos Trans Math Phys Eng Sci* 370(1972):3638–3657.
40. Turner DB, Wilk KE, Curmi PMG, Scholes GD (2011) Comparison of electronic and vibrational coherence measured by two-dimensional electronic spectroscopy. *J. Phys. Chem. Lett.* 2(15):1904–1911.
41. Zhang WM, Meier T, Chernyak V, Mukamel S (1998) Exciton-migration and three-pulse femtosecond optical spectroscopies of photosynthetic antenna complexes. *J Chem Phys* 108:7763.
42. Mukamel S (1995) *Principles of Nonlinear Optical Spectroscopy* (Oxford Univ Press, New York).
43. Won Y, Friesner RA (1988) Theoretical study of photochemical hole burning in photosynthetic bacterial reaction centers. *J Phys Chem* 92(8):2208–2214.
44. Novoderezhkin VI, Dekker JP, van Grondelle R (2007) Mixing of exciton and charge-transfer states in Photosystem II reaction centers: Modeling of Stark spectra with modified Redfield theory. *Biophys J* 93(4):1293–1311.
45. Romero E, van Stokkum IHM, Novoderezhkin VI, Dekker JP, van Grondelle R (2010) Two different charge separation pathways in photosystem II. *Biochemistry* 49(20): 4300–4307.
46. Novoderezhkin VI, Romero E, Dekker JP, van Grondelle R (2011) Multiple charge-separation pathways in photosystem II: Modeling of transient absorption kinetics. *ChemPhysChem* 12(3):681–688.
47. Cardona T, Sedoud A, Cox N, Rutherford AW (2012) Charge separation in photosystem II: A comparative and evolutionary overview. *Biochim Biophys Acta* 1817(1): 26–43.
48. Holzwarth AR, et al. (2006) Kinetics and mechanism of electron transfer in intact photosystem II and in the isolated reaction center: Pheophytin is the primary electron acceptor. *Proc Natl Acad Sci USA* 103(18):6895–6900.
49. Renger T, Schlodder E (2010) Primary photophysical processes in photosystem II: Bridging the gap between crystal structure and optical spectra. *ChemPhysChem* 11(6):1141–1153.
50. Power EA (1964) *Introductory Quantum Electrodynamics* (Elsevier, New York).
51. Lee H, Cheng YC, Fleming GR (2007) Coherence dynamics in photosynthesis: Protein protection of excitonic coherence. *Science* 316(5830):1462–1465.
52. Faist J, Capasso F, Sirtori C, West KW, Pfeiffer LN (1997) Controlling the sign of quantum interference by tunneling from quantum wells. *Nature* 390:589.
53. dell'Orto T, Almeida J, Coluzza C, Margaritondo G, Margaritondo G; Di Ventra M (1995) Evidence for a photocurrent Fano resonance in an artificial nanostructure. *Phys Rev B Condens Matter* 52(4):R2265–R2268.

Supporting Information

Dorfman et al. 10.1073/pnas.1212666110

SI Quantum Master Equation for a Single Two-Level System Coupled to a Harmonic Bath

We now present a microscopic derivation of the quantum master equation (QME)—the main tool for computing the system evolution. Note that the QME is a fully microscopic theory with no phenomenological ansatz. All parameters are determined by the characteristics of the system and the bath.

We consider a single two-level system with a ground b and an excited a eigenstate interacting with light that is represented by a harmonic bath. We study spontaneous and stimulated emission in such a system generated by broadband incoherent thermal radiation. The total Hamiltonian in the dipole approximation is given by

$$\hat{H} = \hat{H}_S + \hat{H}_B + \hat{H}_{SB}, \qquad \text{[S1]}$$

where the two-level system Hamiltonian H_S can be expressed in terms of the system transition operators as

$$\hat{H}_S = \hbar\omega_a |a\rangle\langle a| + \hbar\omega_b |b\rangle\langle b|, \qquad \text{[S2]}$$

where $\hbar\omega_a$ and $\hbar\omega_b$ are eigenstate energies. Introducing $\hat{S}_z = |a\rangle\langle a| - |b\rangle\langle b|$, $\hat{S} = |b\rangle\langle a|$, and $\hat{S}^\dagger = |a\rangle\langle b|$ and taking into account that $\hbar\omega_a|a\rangle\langle a| + \hbar\omega_b|b\rangle\langle b| = \frac{1}{2}\hbar\omega(|a\rangle\langle a| - |b\rangle\langle b|) + \frac{1}{2}\hbar(\omega_a + \omega_b)$. where we define the transition frequency $\hbar\omega = \hbar\omega_a - \hbar\omega_b$ and use $|a\rangle\langle a| + |b\rangle\langle b| = 1$, Eq. **S2** yields

$$\hat{H}_S \simeq \frac{1}{2}\hbar\omega\hat{S}_z, \qquad \text{[S3]}$$

where we have neglected the constant energy term $\hbar(\omega_a + \omega_b)/2$. The Hamiltonian H_B represents a bath of harmonic oscillators

$$\hat{H}_B = \sum_{\mathbf{k}} \hbar\nu_{\mathbf{k}}\hat{a}^\dagger_{\mathbf{k}}\hat{a}_{\mathbf{k}}. \qquad \text{[S4]}$$

The system–bath interaction Hamiltonian is given by the standard $|e|\mathbf{r}\cdot\mathbf{E}$ Hamiltonian, which can be written in the dipole approximation as

$$\hat{H}_{SB} = \hbar\sum_{\mathbf{k}} g_{\mathbf{k}}\left(\hat{S} + \hat{S}^\dagger\right)\left(\hat{a}_{\mathbf{k}} + \hat{a}^\dagger_{\mathbf{k}}\right), \qquad \text{[S5]}$$

where the system–bath coupling constant $g_{\mathbf{k}} = \mathcal{P}_{ab}\cdot\hat{\boldsymbol{\epsilon}}_{\mathbf{k}}\mathcal{E}_{\mathbf{k}}/\hbar$ with the dipole moment of $a \leftrightarrow b$ transition given by $\mathcal{P}_{ab}$ and polarization of the field $\hat{\boldsymbol{\epsilon}}_k$; the electric field per photon is $\mathcal{E}_{\mathbf{k}} = (\hbar\nu_{\mathbf{k}}/2\epsilon_0 V_{\rm ph})^{1/2}$, where $V_{\rm ph}$ is the photon volume. Eq. **S5** yields, after using the rotating-wave approximation (RWA),

$$\hat{H}_{SB} = \hbar\sum_{\mathbf{k}} g_{\mathbf{k}}\left(\hat{S}\hat{a}^\dagger_{\mathbf{k}} + \hat{S}^\dagger\hat{a}_k\right). \qquad \text{[S6]}$$

It is convenient to work in the interaction picture, where the Hamiltonian is transformed as

$$\hat{V} = e^{i\left(\hat{H}_S+\hat{H}_B\right)t/\hbar}\hat{H}_{SB}e^{-i\left(\hat{H}_S+\hat{H}_B\right)t/\hbar}. \qquad \text{[S7]}$$

This gives

$$\hat{V}(t) = \hbar\sum_{\mathbf{k}} g_k\hat{a}_{\mathbf{k}}e^{i(\omega_0-\nu_k)t}\hat{S}^\dagger + \text{H.c.}, \qquad \text{[S8]}$$

where $\omega_0 = E_a - E_b$ is the transition frequency; $\hat{S} \equiv |b\rangle\langle a|$ and $S^\dagger \equiv |a\rangle\langle b|$ are eigenstate lowering and raising operators, respectively. The equation of motion for the density operator $\hat{\rho}$ is (1)

$$\frac{d\hat{\rho}(t)}{dt} = -\frac{i}{\hbar}\text{Tr}_R\left[\hat{V}(t), \hat{\rho}(t_0)\otimes\hat{\rho}_R(t_0)\right] - \frac{1}{\hbar^2}\text{Tr}_R\int_{t_0}^{t}\left[\hat{V}(t), \left[\hat{V}(t'), \hat{\rho}(t')\otimes\hat{\rho}_R(t_0)\right]\right]dt'. \qquad \text{[S9]}$$

Inserting $\hat{V}(t)$ into Eq. **S9**, we recall that $\langle\hat{a}_{\mathbf{k}}\rangle = \langle\hat{a}^+_{\mathbf{k}}\rangle = 0$ and $\langle\hat{a}_{\mathbf{k}}\hat{a}_{\mathbf{k}'}\rangle = \langle\hat{a}^+_{\mathbf{k}}\hat{a}^+_{\mathbf{k}'}\rangle = 0$, where $\langle\hat{A}\rangle$ stands for tracing over the bath $\text{Tr}_R[\hat{\rho}_R(t_0)\hat{A}]$. We next note that

$$\langle\hat{a}^+_{\mathbf{k}}\hat{a}_{\mathbf{k}'}\rangle = \overline{n}_{\mathbf{k}}\delta_{\mathbf{k}\mathbf{k}'}, \qquad \langle\hat{a}_{\mathbf{k}}\hat{a}^+_{\mathbf{k}'}\rangle = (\overline{n}_{\mathbf{k}} + 1)\delta_{\mathbf{k}\mathbf{k}'}.$$

Furthermore, the trace can be easily performed by appropriate cyclic permutations of the operators. The sum over $\mathbf{k}$ can be replaced by the integral as follows:

$$\sum_{\mathbf{k}} \to \frac{V_{\rm ph}}{\pi^2}\int_0^\infty dkk^2.$$

Hereafter we neglect all memory effects in the system (Markov approximation) and assume that $\hat{\rho}(t')$ is a slowly varying function of time. We can thus extend the integration over t' to ∞ and use

$$\int_{t_0}^{\infty} dt' e^{i(\omega-\nu_k)(t-t')} = \pi\delta(\omega - \nu_k).$$

This gives the final form of the QME

$$\dot{\rho} = -\frac{V_{ph}}{c\pi}k_0^2 g^2_{k_0}\left[(\overline{n}_{k_0}+1)\left(\hat{S}^\dagger\hat{S}\rho - 2\hat{S}\rho\hat{S}^\dagger + \rho\hat{S}^\dagger\hat{S}\right) + \overline{n}_{k_0}\left(\hat{S}\hat{S}^\dagger\rho - 2\hat{S}^\dagger\rho\hat{S} + \rho\hat{S}\hat{S}^\dagger\right)\right], \qquad \text{[S10]}$$

where $k_0 = \omega_0/c$. Taking matrix elements of the density operator $\rho_{ij} \equiv \langle i|\rho|j\rangle$ yields

$$\dot{\rho}_{aa} = -\gamma\left[(\overline{n}+1)\rho_{aa} - \overline{n}\rho_{bb}\right], \qquad \rho_{aa} + \rho_{bb} = 1, \qquad \text{[S11]}$$

$$\dot{\rho}_{ab} = -\gamma(\overline{n} + 1/2)\rho_{ab}, \qquad \text{[S12]}$$

where

$$\gamma = \frac{2k_0^2 V_{\rm ph} g^2_{k_0}}{\pi c} \qquad \text{[S13]}$$

is the rate of spontaneous emission for $a \leftrightarrow b$. The average number of photons $\overline{n} \equiv \overline{n}_{k_0}$ for the thermal field at temperature T is given by the Planck distribution

$$\overline{n} = \frac{1}{\exp(\hbar\omega_0/k_BT) - 1}. \qquad \text{[S14]}$$

This form of the QME obtained in the RWA is guaranteed to yield a physically acceptable evolution which always gives positive values for populations (2). By using the RWA, we omit the

counter-rotating terms, i.e., neglecting another type of virtual process such as radiative (Lamb) shift of the energy levels.

SI Four-Level Laser QHE: Density Matrix Analysis

Next we study the model of a laser QHE represented by a four-level system (Fig. S1). Transitions $b \leftrightarrow a$ and $b \leftrightarrow \beta$, $a \leftrightarrow \alpha$ are driven by hot and cold light, respectively. Lasing transition $\alpha \leftrightarrow \beta$ emits coherent laser radiation with power P_l and with energy $\hbar\nu_l = E_\alpha - E_\beta$. Thus, for the four-level laser QHE scheme, the density matrix equations are given by

$$\dot{\rho}_{aa} = -\gamma_c\left[(1+\overline{n}_c)\rho_{aa} - \overline{n}_c\rho_{\alpha\alpha}\right] - \gamma_h\left[(1+\overline{n}_h)\rho_{aa} - \overline{n}_h\rho_{bb}\right], \quad \textbf{[S15]}$$

$$\dot{\rho}_{\alpha\alpha} = \gamma_c\left[(1+\overline{n}_c)\rho_{aa} - \overline{n}_c\rho_{\alpha\alpha}\right] - \frac{P_l}{\hbar\nu_l}, \quad \textbf{[S16]}$$

$$\dot{\rho}_{\beta\beta} = \frac{P_l}{\hbar\nu_l} - \Gamma_c\left[(1+\overline{N}_c)\rho_{\beta\beta} - \overline{N}_c\rho_{bb}\right], \quad \textbf{[S17]}$$

$$\rho_{aa} + \rho_{bb} + \rho_{\alpha\alpha} + \rho_{\beta\beta} = 1. \quad \textbf{[S18]}$$

The laser power P_l is given by

$$\frac{P_l}{\hbar\nu_l} = \frac{g^2}{\gamma_l}\left[(1+\overline{n}_l)\rho_{\alpha\alpha} - \overline{n}_l\rho_{\beta\beta}\right], \quad \textbf{[S19]}$$

where g is the atom–field coupling constant, γ_l is the spontaneous decay rate at the lasing transition $\alpha \leftrightarrow \beta$, and γ_h, γ_c, and Γ_c are the spontaneous decay rates

$$\gamma_h = \frac{2k_{ab}^2\, V_{\rm pht} g_{k_{ab}}^2}{\pi c}, \quad \gamma_c = \frac{2k_{a\alpha}^2\, V_{\rm phn} \tilde{g}_{k_{a\alpha}}^2}{\pi c}, \quad \Gamma_c = \frac{2k_{\beta b}^2\, V_{\rm phn} \tilde{G}_{k_{\beta b}}^2}{\pi c}, \quad \textbf{[S20]}$$

with $V_{\rm pht}$ and $V_{\rm phn}$ representing the photon and phonon volumes, respectively. The average occupation number of photons n at energy $E_{ab} = E_a - E_b$ is given by

$$\overline{n}_h = \frac{1}{\exp\left(\dfrac{E_{ab}}{k_B T_S}\right) - 1}, \quad \textbf{[S21]}$$

whereas $\overline{n}_c$ and $\overline{N}_c$, the average occupation numbers of phonons at energies $E_{a\alpha} = E_a - E_\alpha$ and $E_{\beta b} = E_\beta - E_b$, respectively, are given by

$$\overline{n}_c = \frac{1}{\exp\left(\dfrac{E_{a\alpha}}{k_B T_a}\right) - 1}, \quad \overline{N}_c = \frac{1}{\exp\left(\dfrac{E_{\beta b}}{k_B T_a}\right) - 1}. \quad \textbf{[S22]}$$

The mean number of laser photons $\overline{n}_l$ obeys the equation of motion

$$\dot{\overline{n}}_l = \frac{g^2}{\gamma_l}(\rho_{\alpha\alpha} - \rho_{\beta\beta})\overline{n}_l - \frac{\nu_l}{Q}\overline{n}_l, \quad \textbf{[S23]}$$

where Q is the cavity Q factor. We solve Eqs. **S15**–**S23** for a strong laser field ($\overline{n}_l \gg 1$). For a weak ambient pump $\overline{n}_c \ll 1$ and $\overline{N}_c \ll 1$ in the good cavity limit $g^2 Q/\nu_l\gamma_l \gg 1$, the laser power yields

$$P_l = \frac{\overline{n}_h}{(\gamma_c+\gamma_h)\Gamma_c + 2(\gamma_c+\Gamma_c)\gamma_h\overline{n}_h}\gamma_c\Gamma_c\gamma_h\hbar\nu_l. \quad \textbf{[S24]}$$

The laser threshold condition is determined by equating the populations of the upper and lower laser levels $\rho_{\alpha\alpha} = \rho_{\beta\beta}$. For $n_l \gg 1$ in the good cavity limit, this requirement implies zero laser power $P_l = 0$. In this case Eq. **S16** yields

$$\frac{\rho_{\alpha\alpha}}{\rho_{aa}} = 1 + \frac{1}{\overline{n}_c} = e^{E_{a\alpha}/k_B T_c}. \quad \textbf{[S25]}$$

Substituting the latter result into Eq. **S15** yields

$$\frac{\rho_{aa}}{\rho_{bb}} = \frac{\overline{n}_h}{\overline{n}_h + 1} = e^{-E_{ab}/k_B T_h}. \quad \textbf{[S26]}$$

Similarly, Eq. **S17** at $P_l = 0$ implies

$$\frac{\rho_{bb}}{\rho_{\beta\beta}} = 1 + \frac{1}{\overline{N}_c} = e^{E_{\beta b}/k_B T_c}. \quad \textbf{[S27]}$$

Summarizing the results of Eqs. **S25**–**S27** yields

$$1 = \frac{\rho_{\alpha\alpha}}{\rho_{\beta\beta}} = \frac{\rho_{\alpha\alpha}}{\rho_{aa}}\frac{\rho_{aa}}{\rho_{bb}}\frac{\rho_{bb}}{\rho_{\beta\beta}} = \exp\left(\frac{E_a - E_\alpha + E_\beta - E_b}{k_B T_c} - \frac{E_a - E_b}{k_B T_h}\right), \quad \textbf{[S28]}$$

which is equivalent to the familiar Scovil–Schultz-DuBois result

$$\hbar\nu_l = \hbar\nu_h\left(1 - \frac{T_c}{T_h}\right), \quad \textbf{[S29]}$$

where we take $\hbar\nu_h = E_a - E_b$.

SI Photocell QHE: Maximum Current Delivered to the Load

We note that the simple analysis above can be applied to the photocell QHE by replacing the laser power term $P_l/\hbar\nu_l$ by the cell current j/e. The latter gives the current–voltage characteristics of a photocell similar to those of a p-n junction with internal resistance:

$$\frac{j}{e} = \frac{1 - \exp\left[\dfrac{e(V - V_{oc})}{kT_c}\right]}{C + D\exp\left[\dfrac{e(V - V_{oc})}{kT_c}\right]}, \quad \textbf{[S30]}$$

where the open-circuit voltage V_{oc} is given by

$$eV_{oc} = (E_a - E_b)\left(1 - \frac{T_c}{T_h}\right). \quad \textbf{[S31]}$$

The factor C has the meaning of the reverse saturation current j_0, whereas D/C is equivalent to $j_0 eR/kT_c$, where R is the internal cell resistance. The general solutions for C and D are given in ref. 3. In the limit of a weak ambient pump ($\overline{n}_c \ll 1$, $\overline{N}_c \ll 1$), the maximum current is given by

$$j/e = \frac{\gamma_c\Gamma_c\gamma_h\overline{n}_h}{\gamma_c\Gamma_c + (\gamma_c + 2\Gamma_c)\gamma_h\overline{n}_h}. \quad \textbf{[S32]}$$

SI Simplest Model of the Biological Quantum Heat Engine

The simplest biological quantum heat engine (BQHE) consists of two interacting molecules. The states a, b, α, and β form the full set of two-body states that provide the charge separation. Solar radiation (photon heat bath) drives transitions from b to a, whereas low-entropy sink (phonon bath) couples a to α and b to β. The system Hamiltonian for a two-body model, neglecting the Lamb shift, can be written as $\hat{H}_S = \hbar\sum_j \omega_j |j\rangle\langle j|$ ($j = a, b, \alpha, \beta$). Similarly, the system–bath interaction Hamiltonian can be described by

$$\hat{H}_{SB} = \hbar\sum_{\mathbf{k}} g_{\mathbf{k}}\hat{a}_{\mathbf{k}}^\dagger|b\rangle\langle a| + \hbar\sum_{\mathbf{q}}\tilde{g}_{\mathbf{q}}\hat{b}_{\mathbf{q}}^\dagger|\alpha\rangle\langle a| + \hbar\sum_{\mathbf{p}}\tilde{G}_{\mathbf{p}}\hat{c}_{\mathbf{p}}^\dagger|b\rangle\langle\beta| + \text{H.c.}, \quad \textbf{[S33]}$$

where the creation operator $\hat{a}_{\mathbf{k}}^\dagger$ couples the optical transition $a \leftrightarrow b$ with the emission of a photon with the momentum $\hbar\mathbf{k}$,

whereas the phonons with momenta $\hbar\mathbf{q}$ and $\hbar\mathbf{p}$ created by the operators $\hat{b}^{\dagger}_{\mathbf{q}}$ and $\hat{c}^{\dagger}_{\mathbf{p}}$ drive the low-temperature transitions $a \leftrightarrow \alpha$ and $\beta \leftrightarrow b$, respectively. In addition, we assume that reservoir states α and β are connected through the membranes (4) and we model the population transfer between them in the QME by introducing rate Γ. The evolution of density matrix elements reads

$$\dot{\rho}_{aa} = \gamma_h\left[\overline{n}_h\rho_{bb} - \left(\overline{n}_h+1\right)\rho_{aa}\right] + \gamma_c\left[\overline{n}_c\rho_{\alpha\alpha} - \left(\overline{n}_c+1\right)\rho_{aa}\right], \quad \textbf{[S34]}$$

$$\dot{\rho}_{\alpha\alpha} = \gamma_c\left[\left(\overline{n}_c+1\right)\rho_{aa} - \overline{n}_c\rho_{\alpha\alpha}\right] - \Gamma\rho_{\alpha\alpha}, \quad \textbf{[S35]}$$

$$\dot{\rho}_{\beta\beta} = \Gamma\rho_{\alpha\alpha} + \Gamma_c\left[\overline{N}_c\rho_{bb} - \left(\overline{N}_c+1\right)\rho_{\beta\beta}\right], \quad \textbf{[S36]}$$

$$\rho_{aa} + \rho_{bb} + \rho_{\alpha\alpha} + \rho_{\beta\beta} = 1. \quad \textbf{[S37]}$$

Eqs. **S34**–**S37** allow us to calculate the dynamics of populations of the charge-separated states. On the other hand, in the long time limit, one can study the steady-state characteristics of the QHE, such as the electron flux j or the electrostatic potential across the membranes.

SI Noise-Induced Population–Coherence Coupling: Simplest Amplitude Treatment

In this section, we consider a simple example of the manifestation of virtual processes and quantum interference in a three-level system: the Agarwal–Fano coupling (5) for a simple problem of radiative decay of $|a_1\rangle$ and $|a_2\rangle$ levels in the ground state $|b\rangle$ with the emission of a photon of wave vector $\mathbf{k}$. The interaction picture Hamiltonian in the RWA for this system coupled to a harmonic bath is

$$H_{SB} = \hbar\sum_{\mathbf{k}}\left[g^{*}_{1\mathbf{k}}\hat{S}^{\dagger}_{1}\hat{a}_{\mathbf{k}}e^{i(\omega_1-\nu_{\mathbf{k}})t} + g^{*}_{2\mathbf{k}}\hat{S}^{\dagger}_{2}\hat{a}_{\mathbf{k}}e^{i(\omega_2-\nu_{\mathbf{k}})t} + \text{H.c.}\right], \quad \textbf{[S38]}$$

where $\hat{S}^{\dagger}_{j} \equiv \sigma^{+}_{a_j b} = \sigma_{j x} + i\sigma_{j y}$, $j = 1, 2$ is the material system raising Pauli operator; $a_{\mathbf{k}}$ is the annihilation operator of a photon with momentum $\hbar\mathbf{k}$; and $g_{j\mathbf{k}}$ is the coupling constant for the $|a_j, 0\rangle \rightarrow |b, 1_{\mathbf{k}}\rangle$ transition. The time-dependent state vector for the system is given by

$$|\psi\rangle = \alpha_1(t)|a_1, 0\rangle + \alpha_2(t)|a_2, 0\rangle + \sum_{\mathbf{k}}\beta_{\mathbf{k}}(t)|b, 1_{\mathbf{k}}\rangle, \quad \textbf{[S39]}$$

where $|0\rangle$ and $|1_{\mathbf{k}}\rangle$ are the vacuum and single photon states, respectively. The Schrödinger equation for the probability amplitudes α_1, α_2, and $\beta_{\mathbf{k}}$ yields

$$\dot{\alpha}_1(t) = -i\sum_{\mathbf{k}} g^{*}_{1\mathbf{k}}\beta_{\mathbf{k}}e^{i(\omega_{1b}-\nu_{\mathbf{k}})t}, \quad \textbf{[S40]}$$

$$\dot{\alpha}_2(t) = -i\sum_{\mathbf{k}} g^{*}_{2\mathbf{k}}\beta_{\mathbf{k}}e^{i(\omega_{2b}-\nu_{\mathbf{k}})t}, \quad \textbf{[S41]}$$

$$\dot{\beta}_{\mathbf{k}}(t) = -ig_{1\mathbf{k}}\alpha_1 e^{-i(\omega_{1b}-\nu_{\mathbf{k}})t} - ig_{2\mathbf{k}}\alpha_2 e^{-i(\omega_{2b}-\nu_{\mathbf{k}})t}, \quad \textbf{[S42]}$$

where $\hbar\omega_{ib} = E_{a_i} - E_b$ is the energy spacing between levels $|a_i\rangle$ and $|b\rangle$, and $\nu_{\mathbf{k}}$ is the photon frequency. We proceed by integrating Eq. **S42** and substituting the result into Eqs. **S40** and **S41** Using the Weisskopf–Wigner approximation (1) we find

$$\dot{\alpha}_1 = -\frac{\gamma_1}{2}\alpha_1 - \frac{\sqrt{\gamma_1\gamma_2}}{2}\alpha_2 e^{i\Delta t}, \quad \textbf{[S43]}$$

$$\dot{\alpha}_2 = -\frac{\gamma_2}{2}\alpha_2 - \frac{\sqrt{\gamma_1\gamma_2}}{2}\alpha_1 e^{-i\Delta t}, \quad \textbf{[S44]}$$

where

$$\gamma_i = \frac{1}{4\pi\epsilon_0}\frac{4\omega^3_{ib}\mathcal{P}^2_{ib}}{3\hbar c^3} \quad \textbf{[S45]}$$

is the radiative decay rate of the transition $|a_i\rangle \rightarrow |b\rangle$ with a corresponding frequency ω_I; a dipole moment $\mathcal{P}_{ib}$; $\Delta = \omega_{1b} - \omega_{2b}$ is the level spacing between $|a_1\rangle$ and $|a_2\rangle$. Furthermore, Eqs. **S43** and **S44** are equivalent to the following density matrix equations (ref. 6):

$$\dot{\rho}_{11} = -\gamma_1\rho_{11} - \frac{1}{2}\sqrt{\gamma_1\gamma_2}\left(\tilde{\rho}_{12} + \tilde{\rho}_{21}\right), \quad \textbf{[S46]}$$

$$\dot{\rho}_{22} = -\gamma_2\rho_{22} - \frac{1}{2}\sqrt{\gamma_1\gamma_2}\left(\tilde{\rho}_{12} + \tilde{\rho}_{21}\right), \quad \textbf{[S47]}$$

$$\dot{\tilde{\rho}}_{12} = -\frac{1}{2}(\gamma_1+\gamma_2)\tilde{\rho}_{12} - i\Delta\tilde{\rho}_{12} - \frac{1}{2}\sqrt{\gamma_1\gamma_2}(\rho_{11}+\rho_{22}), \quad \textbf{[S48]}$$

where ρ_{ii} and $\tilde{\rho}_{ij} \equiv \rho_{ij}e^{i\Delta t}$ $(i \neq j)$ represent the diagonal (populations) and off-diagonal (coherences) matrix elements, respectively.

Expressions **S46**–**S48** apply to the simple case of degenerate levels, i.e., $\omega_{1b} = \omega_{2b}$ and real matrix elements $(g_{i\mathbf{k}} = g^{*}_{i\mathbf{k}})$. Physically the interference terms $\sqrt{\gamma_1\gamma_2}$ are the results of the virtual emission and reabsorption of radiation such as $|a_1, 0\rangle \rightarrow |b, 1_{\mathbf{k}}\rangle \rightarrow |a_2, 0\rangle$, etc. Virtual processes due to quantum noise that are the source of the quantum interference at zero temperature become less subtle at finite temperature, when thermal noise leads to stimulated emission and absorption as an additional channel of interference (3). Furthermore, noise-induced coherence can be created in a system with two lower levels by stimulated absorption and reemission of a virtual photon (3). In the following we consider a more general model that includes both noise-induced coherence and electron transport.

SI Microscopic Derivation of the QME with Couplings Between Populations and Coherences

Next, we derive the master equation that reveals coupling between populations and coherences due to noise. For simplicity we focus on a three-level system with eigenstates 1, 2, and b. The two upper levels 1 and 2 have frequencies ω_1 and ω_2. Following the general approach outlined in *SI QME for a Single Two-Level System Coupled to a Harmonic Bath*, we transform the system and bath Hamiltonians. Thus, in the interaction picture and the RWA, the system–bath Hamiltonian reads

$$\hat{V}(t) = \hbar\sum_{\mathbf{k}} g_{1k}\hat{a}_{\mathbf{k}}e^{i(\omega_1-\nu_k)t}\hat{S}^{\dagger}_{1} + \hbar\sum_{\mathbf{q}} g_{2q}\hat{a}_{\mathbf{q}}e^{i(\omega_2-\nu_q)t}\hat{S}^{\dagger}_{2} + \text{H.c.}, \quad \textbf{[S49]}$$

where $g_{ik} = \sqrt{\hbar\nu_k/\epsilon_0 V}\mathcal{P}_i$ are the atom–radiation coupling constants corresponding to dipole transitions with the strength $\mathcal{P}_i$ $(i = 1, 2)$, whereas $\hat{S}^{\dagger}_{1}(\hat{S}_1)$ and $\hat{S}^{\dagger}_{2}(\hat{S}_2)$ are the raising (lowering) operators for transitions between eigenstates $b \leftrightarrow 1$ and $b \leftrightarrow 2$, respectively $(\hat{S}^{\dagger}_{i} \equiv |i\rangle\langle b|, \hat{S}_i \equiv |b\rangle\langle i|, i = 1, 2)$. We assume that the system interacts with a thermal reservoir described by the density operator $\hat{\rho}_R$. Substituting $\hat{V}(t)$ into Eq. **S9**, we find the QME for the density operator

$$\frac{d\hat{\rho}(t)}{dt} = -\int_{t_0}^{t} dt' \Bigg\{ \sum_{\mathbf{k},\mathbf{k}'} g_{1k} g_{1k'} e^{i(\omega_1-\nu_k)t - i(\omega_1-\nu_{k'})t'} \mathrm{Tr}_R \left[\hat{a}_{\mathbf{k}} \hat{S}_1^\dagger, \left[\hat{a}_{\mathbf{k}'}^+ \hat{S}_1, \hat{\rho}(t') \otimes \hat{\rho}_R(t_0) \right] \right]$$
$$+ \sum_{\mathbf{k},\mathbf{q}'} g_{1k} g_{2q'} e^{i(\omega_1-\nu_k)t - i(\omega_2-\nu_{q'})t'} \mathrm{Tr}_R \left[\hat{a}_{\mathbf{k}} \hat{S}_1^\dagger, \left[\hat{a}_{\mathbf{q}'}^+ \hat{S}_2, \hat{\rho}(t') \otimes \hat{\rho}_R(t_0) \right] \right] + \sum_{\mathbf{q},\mathbf{k}'} g_{2q} g_{1k'} e^{i(\omega_2-\nu_q)t - i(\omega_1-\nu_{k'})t'} \mathrm{Tr}_R \left[\hat{a}_{\mathbf{q}} \hat{S}_2^\dagger, \left[\hat{a}_{\mathbf{k}'}^+ \hat{S}_1, \hat{\rho}(t') \otimes \hat{\rho}_R(t_0) \right] \right]$$
$$+ \sum_{\mathbf{q},\mathbf{q}'} g_{2q} g_{2q'} e^{i(\omega_2-\nu_q)t - i(\omega_2-\nu_{q'})t'} \mathrm{Tr}_R \left[\hat{a}_{\mathbf{q}} \hat{S}_2^\dagger, \left[\hat{a}_{\mathbf{q}'}^+ \hat{S}_2, \hat{\rho}(t') \otimes \hat{\rho}_R(t_0) \right] \right] + \sum_{\mathbf{k},\mathbf{k}'} g_{1k} g_{1k'} e^{-i(\omega_1-\nu_k)t + i(\omega_1-\nu_{k'})t'} \mathrm{Tr}_R \left[\hat{a}_{\mathbf{k}}^+ \hat{S}_1, \left[\hat{a}_{\mathbf{k}'} \hat{S}_1^\dagger, \hat{\rho}(t') \otimes \hat{\rho}_R(t_0) \right] \right]$$
$$+ \sum_{\mathbf{k},\mathbf{q}'} g_{1k} g_{2q'} e^{-i(\omega_1-\nu_k)t + i(\omega_2-\nu_{q'})t'} \mathrm{Tr}_R \left[\hat{a}_{\mathbf{k}}^+ \hat{S}_1, \left[\hat{a}_{\mathbf{q}'} \hat{S}_2^\dagger, \hat{\rho}(t') \otimes \hat{\rho}_R(t_0) \right] \right] + \sum_{\mathbf{q},\mathbf{k}'} g_{2q} g_{1k'} e^{-i(\omega_2-\nu_q)t + i(\omega_1-\nu_{k'})t'} \mathrm{Tr}_R \left[\hat{a}_{\mathbf{q}}^+ \hat{S}_2, \left[\hat{a}_{\mathbf{k}'} \hat{S}_1^\dagger, \hat{\rho}(t') \otimes \hat{\rho}_R(t_0) \right] \right]$$
$$+ \sum_{\mathbf{q},\mathbf{q}'} g_{2q} g_{2q'} e^{-i(\omega_2-\nu_q)t + i(\omega_2-\nu_{q'})t'} \mathrm{Tr}_R \left[\hat{a}_{\mathbf{q}}^+ \hat{S}_2, \left[\hat{a}_{\mathbf{q}'} \hat{S}_2^\dagger, \hat{\rho}(t') \otimes \hat{\rho}_R(t_0) \right] \right] \Bigg\}. \quad \textbf{[S50]}$$

Following the same procedure outlined for a two-level system interacting with a bath, the QME reduces to

$$\frac{d\hat{\rho}(t)}{dt} = -\frac{V_{\mathrm{ph}}}{c\pi} \Bigg\{ k_1^2 g_{1k_1}^2 \left[(\overline{n}_{k_1}+1) \left(\hat{S}_1^\dagger \hat{S}_1 \rho - \hat{S}_1 \rho \hat{S}_1^\dagger \right) + \overline{n}_{k_1} \left(\rho \hat{S}_1 \hat{S}_1^\dagger - \hat{S}_1^\dagger \rho \hat{S}_1 \right) \right] + k_2^2 g_{1k_2} g_{2k_2} e^{i\Delta t} \left[(\overline{n}_{k_2}+1) \left(\hat{S}_1^\dagger \hat{S}_2 \rho - \hat{S}_2 \rho \hat{S}_1^\dagger \right) - \overline{n}_{k_2} \hat{S}_1^\dagger \rho \hat{S}_2 \right]$$
$$+ k_1^2 g_{2k_1} g_{1k_1} e^{-i\Delta t} \left[(\overline{n}_{k_1}+1) \left(\hat{S}_2^\dagger \hat{S}_1 \rho - \hat{S}_1 \rho \hat{S}_2^\dagger \right) - \overline{n}_{k_1} \hat{S}_2^\dagger \rho \hat{S}_1 \right] + k_2^2 g_{2k_2}^2 \left[(\overline{n}_{k_2}+1) \left(\hat{S}_2^\dagger \hat{S}_2 \rho - \hat{S}_2 \rho \hat{S}_2^\dagger \right) + \overline{n}_{k_2} \left(\rho \hat{S}_2 \hat{S}_2^\dagger - \hat{S}_2^\dagger \rho \hat{S}_2 \right) \right]$$
$$+ k_1^2 g_{1k_1}^2 \left[(\overline{n}_{k_1}+1) \left(\rho \hat{S}_1^\dagger \hat{S}_1 - \hat{S}_1 \rho \hat{S}_1^\dagger \right) + \overline{n}_{k_1} \left(\hat{S}_1 \hat{S}_1^\dagger \rho - \hat{S}_1^\dagger \rho \hat{S}_1 \right) \right] + k_2^2 g_{1k_2} g_{2k_2} e^{-i\Delta t} \left[(\overline{n}_{k_2}+1) \left(\rho \hat{S}_2^\dagger \hat{S}_1 - \hat{S}_1 \rho \hat{S}_2^\dagger \right) - \overline{n}_{k_2} \hat{S}_2^\dagger \rho \hat{S}_1 \right]$$
$$+ k_1^2 g_{2k_1} g_{1k_1} e^{i\Delta t} \left[(\overline{n}_{k_1}+1) \left(\rho \hat{S}_1^\dagger \hat{S}_2 - \hat{S}_2 \rho \hat{S}_1^\dagger \right) - \overline{n}_{k_1} \hat{S}_1^\dagger \rho \hat{S}_2 \right] + k_2^2 g_{2k_2}^2 \left[(\overline{n}_{k_2}+1) \left(\rho \hat{S}_2^\dagger \hat{S}_2 - \hat{S}_2 \rho \hat{S}_2^\dagger \right) + \overline{n}_{k_2} \left(\hat{S}_2 \hat{S}_2^\dagger \rho - \hat{S}_2^\dagger \rho \hat{S}_2 \right) \right] \Bigg\}, \quad \textbf{[S51]}$$

where $k_{1,2} = \omega_{1,2}/c$, and $\Delta = \omega_1 - \omega_2$. Introducing notations

$$\gamma_{ij} = \frac{2k_i^2 V_{\mathrm{ph}}\, g_{ik_i}\, g_{jk_i}}{\pi c}$$

and redefining the density matrix operator $\langle i|\tilde{\rho}|j\rangle = \langle i|\rho|j\rangle e^{i(\omega_i-\omega_j)t}$, the QME becomes

$$\frac{d\tilde{\rho}(t)}{dt} = -i \sum_{i,j=1}^{2} (\omega_i - \omega_j)\tilde{\rho}$$
$$- \sum_{i,j=1}^{2} \gamma_{ij} \Big[(\overline{n}_{k_i}+1) \left(\hat{S}_j^\dagger \hat{S}_i \tilde{\rho} + \rho \hat{S}_i^\dagger \hat{S}_j - \hat{S}_i \tilde{\rho} \hat{S}_j^\dagger - \hat{S}_j \tilde{\rho} \hat{S}_i^\dagger \right)$$
$$+ \overline{n}_{k_i} \left(\hat{S}_i^\dagger \hat{S}_i \tilde{\rho} + \tilde{\rho} \hat{S}_i^\dagger \hat{S}_i - \hat{S}_i^\dagger \tilde{\rho} \hat{S}_j - \hat{S}_j^\dagger \rho \hat{S}_i \right) \Big]. \quad \textbf{[S52]}$$

Thus, the terms that couple population and coherence are presented for $i \neq j$. Because $g_k \sim \sqrt{k}\mathcal{P}\cdot\hat{\boldsymbol{\epsilon}}_k$ is a slowly varying function of k and the level spacing is small ($\omega_1 - \omega_2 \; \omega_{1,2}$), we assume that the matrix $\gamma_{12} \simeq \gamma_{21} = 0$ for no coherence whereas $\gamma_{12} \simeq \gamma_{21} \simeq \sqrt{\gamma_1 \gamma_2}$ for maximum coherence. We take $\gamma_i \equiv \gamma_{ii}$ ($i = 1, 2$) corresponding to the rate of spontaneous emission, i.e., the natural linewidth of the corresponding eigenstate. Taking matrix elements of Eq. **S52** $\rho_{ij} \equiv \langle i|\tilde{\rho}|j\rangle$, we finally obtain

$$\dot{\rho}_{11} = -\gamma_1 \left[(\overline{n}_1+1)\rho_{11} - \overline{n}_1 \rho_{bb} \right] - \frac{\gamma_{12}}{2} (\overline{n}_2+1) \left[\tilde{\rho}_{21} + \tilde{\rho}_{12} \right], \quad \textbf{[S53]}$$

$$\dot{\rho}_{22} = -\gamma_2 \left[(\overline{n}_2+1)\rho_{22} - \overline{n}_2 \rho_{bb} \right] - \frac{\gamma_{12}}{2} (\overline{n}_1+1) \left[\tilde{\rho}_{12} + \tilde{\rho}_{21} \right], \quad \textbf{[S54]}$$

$$\dot{\tilde{\rho}}_{12} = -\frac{1}{2} \left[\gamma_1 (\overline{n}_1+1) + \gamma_2 (\overline{n}_2+1) \right] \tilde{\rho}_{12} - i\Delta\tilde{\rho}_{12}$$
$$- \frac{\gamma_{12}}{2} \left[(\overline{n}_1+1)\rho_{11} + (\overline{n}_2+1)\rho_{22} - (\overline{n}_1+\overline{n}_2)\rho_{bb} \right], \quad \textbf{[S55]}$$

where $\tilde{\rho}_{12} = \rho_{12} e^{-i\Delta t}$ with $\Delta = \omega_1 - \omega_2$, and $\overline{n}_i \equiv \overline{n}_{k_i}$ ($i = 1, 2$).

SI Laser QHE Enhanced by Noise-Induced Coherence

Consider a laser model with the upper state a replaced by a doublet a_1 and a_2 (Fig. S2). Based on the analysis given in *SI Microscopic Derivation of the QME with Couplings Between Populations and Coherences* and taking into account the noise-induced coherence as per Eqs. **S53**–**S55**, the evolution of the density matrix elements for the laser QHE with degenerate upper levels a_1, a_2 ($\Delta = 0$) is described by

$$\dot{\rho}_{11} = -\gamma_{1c} \left[(1+\overline{n}_c)\rho_{11} - \overline{n}_c \rho_{\alpha\alpha} \right] - \gamma_{1h} \left[(1+\overline{n}_h)\rho_{11} - \overline{n}_h \rho_{bb} \right]$$
$$- \left[\gamma_{12c} (1+\overline{n}_c) + \gamma_{12h} (1+\overline{n}_h) \right] \mathrm{Re}[\rho_{12}], \quad \textbf{[S56]}$$

$$\dot{\rho}_{22} = -\gamma_{2c} \left[(1+\overline{n}_c)\rho_{22} - \overline{n}_c \rho_{\alpha\alpha} \right] - \gamma_{2h} \left[(1+\overline{n}_h)\rho_{22} - \overline{n}_h \rho_{bb} \right]$$
$$- \left[\gamma_{12c} (1+\overline{n}_c) + \gamma_{12h} (1+\overline{n}_h) \right] \mathrm{Re}[\rho_{12}], \quad \textbf{[S57]}$$

$$\dot{\rho}_{12} = -\frac{1}{2}\left[(\gamma_{1h}+\gamma_{2h})(1+\overline{n}_h)+(\gamma_{1c}+\gamma_{2c})(1+\overline{n}_c)\right]\rho_{12} - \frac{\gamma_{12c}}{2}\left[(1+\overline{n}_c)(\rho_{11}+\rho_{22})-2\overline{n}_c\rho_{\alpha\alpha}\right] - \frac{\gamma_{12h}}{2}\left[(1+\overline{n}_h)(\rho_{11}+\rho_{22})-2\overline{n}_h\rho_{bb}\right]-\frac{\rho_{12}}{\tau_2}, \quad \textbf{[S58]}$$

$$\dot{\rho}_{\alpha\alpha} = \gamma_{1c}\left[(1+\overline{n}_c)\rho_{11}-\overline{n}_c\rho_{\alpha\alpha}\right]+\gamma_{2c}\left[(1+\overline{n}_c)\rho_{22}-\overline{n}_c\rho_{\alpha\alpha}\right] + 2\gamma_{12c}(1+\overline{n}_c)\mathrm{Re}[\rho_{12}]-\frac{P_l}{\hbar\nu_l}, \quad \textbf{[S59]}$$

$$\dot{\rho}_{\beta\beta} = \frac{P_l}{\hbar\nu_l}-\Gamma_c\left[(1+\overline{N}_c)\rho_{\beta\beta}-\overline{N}_c\rho_{bb}\right], \quad \textbf{[S60]}$$

$$\rho_{11}+\rho_{22}+\rho_{aa}+\rho_{\beta\beta}=1. \quad \textbf{[S61]}$$

The maximum interference corresponds to $\gamma_{12h}=\sqrt{\gamma_{1h}\gamma_{2h}}$ and $\gamma_{12c}=\sqrt{\gamma_{1c}\gamma_{2c}}$, whereas for no interference $\gamma_{12h}=\gamma_{12c}=0$. Taking into account Eqs. **S19** and **S23** for $\gamma_{1c}=\gamma_{2c}=\gamma_c$, $\gamma_{1h}=\gamma_{2h}=\gamma_h$, and assuming no decoherence $1/\tau_2=0$, the maximum coherence reads

$$\rho_{12}=\frac{\left[\frac{\gamma_{12c}}{\gamma_c}-\frac{\gamma_{12h}}{\gamma_h}\right]\frac{P_l}{2\hbar\nu_l}}{\gamma_c(1+\overline{n}_c)\left[1-\left(\frac{\gamma_{12c}}{\gamma_c}\right)^2\right]+\gamma_h(1+\overline{n}_h)\left[1-\left(\frac{\gamma_{12h}}{\gamma_h}\right)^2\right]}. \quad \textbf{[S62]}$$

In the approximation of a weak ambient pump $\overline{n}_c, \overline{N}_c \ll 1$ in the strong field and good cavity limits, we find the laser power with no coherence to be

$$P_l=\frac{2\overline{n}_h}{(\gamma_c+\gamma_h)\Gamma_c+(4\gamma_c+3\Gamma_c)\gamma_h\overline{n}_h}\gamma_c\Gamma_c\gamma_h\hbar\nu_l, \quad \textbf{[S63]}$$

whereas for the maximum coherence the power is

$$P_l=\frac{2\overline{n}_h}{(\gamma_c+\gamma_h)\Gamma_c+2(2\gamma_c+\Gamma_c)\gamma_h\overline{n}_h}\gamma_c\Gamma_c\gamma_h\hbar\nu_l. \quad \textbf{[S64]}$$

Thus, in the limit of $\gamma_c \ll \Gamma_c \ll \gamma_h\overline{n}_h$, the power of the laser QHE with the single upper level of Eq. **S24** is given by

$$P_l=\frac{1}{2}\gamma_c\hbar\nu_l. \quad \textbf{[S65]}$$

Similarly, the laser power for the model with an upper doublet and no coherence of Eq. **S63** yields a 33% enhancement result

$$P_l=\frac{2}{3}\gamma_c\hbar\nu_l, \quad \textbf{[S66]}$$

whereas for the model with maximum coherence the result of Eq. **S64** compared with the model with a single level yields a result that is 2× larger,

$$P_l=\gamma_c\hbar\nu_l. \quad \textbf{[S67]}$$

SI Photocell QHE Enhanced by Noise-Induced Coherence

Similarly, we consider a photocell QHE with the upper state a replaced by a doublet a_1 and a_2. This model is described by the same equations as the laser QHE (Eqs. **S56–S61**) if one replaces the laser power $P_l/\hbar\nu_l$ by the cell current j/e. The current–voltage characteristics for the coherence-enhanced photocell are also given by Eq. **S30** with different values of factors C and D (3). The coherence ρ_{12} is given by

$$\rho_{12}=\frac{\left[\frac{\gamma_{12c}}{\gamma_c}-\frac{\gamma_{12h}}{\gamma_h}\right]\frac{j}{2e}}{\gamma_c(1+\overline{n}_c)\left[1-\left(\frac{\gamma_{12c}}{\gamma_c}\right)^2\right]+\gamma_h(1+\overline{n}_h)\left[1-\left(\frac{\gamma_{12h}}{\gamma_h}\right)^2\right]}. \quad \textbf{[S68]}$$

For the weak ambient pump $\overline{n}_c, \overline{N}_c \ll 1$, the cell current with no coherence is given by

$$j/e=\frac{2\gamma_c\Gamma_c\gamma_h\overline{n}_h}{\gamma_c\Gamma_c+(2\gamma_c+3\Gamma_c)\gamma_h\overline{n}_h}, \quad \textbf{[S69]}$$

whereas for the maximum coherence it yields

$$j/e=\frac{2\gamma_c\Gamma_c\gamma_h\overline{n}_h}{\gamma_c\Gamma_c+2(\gamma_c+\Gamma_c)\gamma_h\overline{n}_h}. \quad \textbf{[S70]}$$

Thus, for $\gamma_2 \ll \Gamma_c,\gamma_h\overline{n}_h$, Eq. **S32** yields for the model with a single level a

$$j/e=\frac{1}{2}e\gamma_c. \quad \textbf{[S71]}$$

Similarly, for the model with an upper doublet and no coherence we have 33% enhancement

$$j/e=\frac{2}{3}\gamma_c, \quad \textbf{[S72]}$$

and 100% enhancement for the maximum coherence

$$j/e=\gamma_c. \quad \textbf{[S73]}$$

Thus, because the power of the photocell QHE is given by $P_{cell}=j\cdot V$ and the value of the voltage V that corresponds to the maximum power is close to the open-circuit voltage $eV_{oc}=(E_a-E_b)(1-T_c/T_h)$, the power delivered to the load by a photocell is essentially determined by the value of the maximum current and, therefore, can be doubled by inducing coherence.

SI Coherence-Assisted BQHE

To extend the ideas of the previous sections to photosynthesis, we consider a three-body BQHE with two donor and one acceptor molecules. Namely, we note that if two identical donor molecules are close together and absorb sunlight cooperatively, then there exist two exciton states separated by Davydov splitting. We denote them a_1 and a_2. Furthermore, applying the formalism of *SI Simplest Model of the BQHE* to this model yields the following evolution of the density matrix elements ($\rho_{a_ia_j}\equiv\rho_{ij}$):

$$\dot{\rho}_{11} = -\gamma_{12h}(\overline{n}_{2h}+1)\mathrm{Re}[\rho_{12}]-\gamma_{12c}(\overline{n}_{2c}+1)\mathrm{Re}[\rho_{12}] -\gamma_{1h}\left[(\overline{n}_{1h}+1)\rho_{11}-\overline{n}_{1h}\rho_{bb}\right]-\gamma_{1c}\left[(\overline{n}_{1c}+1)\rho_{11}-\overline{n}_{1c}\rho_{\alpha\alpha}\right], \quad \textbf{[S74]}$$

$$\dot{\rho}_{22} = -\gamma_{12h}(\overline{n}_{1h}+1)\mathrm{Re}[\rho_{12}]-\gamma_{12c}(\overline{n}_{1c}+1)\mathrm{Re}[\rho_{12}] -\gamma_{2h}\left[(\overline{n}_{2h}+1)\rho_{22}-\overline{n}_{2h}\rho_{bb}\right]-\gamma_{2c}\left[(\overline{n}_{2c}+1)\rho_{22}-\overline{n}_{2c}\rho_{\alpha\alpha}\right], \quad \textbf{[S75]}$$

$$\dot{\rho}_{12} = -\frac{\gamma_{12h}}{2}\left[(\overline{n}_{1h}+1)\rho_{11} + (\overline{n}_{2h}+1)\rho_{22} - (\overline{n}_{1h}+\overline{n}_{2h})\rho_{bb}\right] - \frac{\gamma_{12c}}{2}\left[(\overline{n}_{1c}+1)\rho_{11} + (\overline{n}_{2c}+1)\rho_{22} - (\overline{n}_{1c}+\overline{n}_{2c})\rho_{\alpha\alpha}\right] - \frac{1}{2}\left[\gamma_{1h}(\overline{n}_{1h}+1) + \gamma_{2h}(\overline{n}_{2h}+1)\right]\rho_{12} - \left(i\Delta + \frac{1}{\tau_2}\right)\rho_{12} - \frac{1}{2}\left[\gamma_{1c}(\overline{n}_{c1}+1) + \gamma_{2c}(\overline{n}_{2c}+1)\right]\rho_{12}, \quad \textbf{[S76]}$$

$$\dot{\rho}_{\alpha\alpha} = \gamma_{12c}(\overline{n}_{1c}+\overline{n}_{2c}+2)\mathrm{Re}[\rho_{12}] - \Gamma\rho_{\alpha\alpha} + \gamma_{1c}\left[(\overline{n}_{1c}+1)\rho_{11} - \overline{n}_{1c}\rho_{\alpha\alpha}\right] + \gamma_{2c}\left[(\overline{n}_{2c}+1)\rho_{22} - \overline{n}_{2c}\rho_{\alpha\alpha}\right], \quad \textbf{[S77]}$$

$$\dot{\rho}_{\beta\beta} = \Gamma\rho_{\alpha\alpha} - \Gamma_c\left[(\overline{N}_c+1)\rho_{\beta\beta} - \overline{N}_c\rho_{bb}\right], \quad \textbf{[S78]}$$

$$\rho_{bb} + \rho_{11} + \rho_{22} + \rho_{\alpha\alpha} + \rho_{\beta\beta} = 1, \quad \textbf{[S79]}$$

where γ_i and $\tilde{\gamma}_i$ are the spontaneous decay rates of the transitions $a_{1,2} \to b$ and $a_{1,2} \to \alpha$, respectively. $\overline{n}_{1h}$, $\overline{n}_{2h}$ and $\overline{n}_{1c}$, $\overline{n}_{2c}$, $\overline{N}_c$ are the photon and phonon occupation numbers similar to $\overline{n}_h$, $\overline{n}_c$, and $\overline{N}_c$ of Eqs. **S21** and **S22** with E_{ab} and $E_{a\alpha}$ replaced by $E_{1,2} - E_b$ and $E_{1,2} - E_\alpha$, respectively; τ_2 is the decoherence time; $\Delta = \omega_1 - \omega_2$ is the splitting of the levels a_1 and a_2. The noise-induced couplings $\gamma_{12h} = \sqrt{\gamma_{1h}\gamma_{2h}}$ and $\gamma_{12c} = \sqrt{\gamma_{1c}\gamma_{2c}}$ for the maximum coherence, whereas for no coherence $\gamma_{12h} = \gamma_{12c} = 0$.

SI Application to the Reaction Center of Photosystem II

We apply the model in the previous section to describe the dynamics of a photosynthetic reaction center (RC) (Fig. S3). Photosynthetic antennae transfer energy of the absorbed solar photons to the RC where the transmembrane charge separation takes place. The resulting electrochemical potential drives the synthesis of ATP and the oxidized part of the RC splits water, releasing molecular oxygen. RCs from green plants, algae, and bacteria have similar overall structures but they differ in the nature and precise orientation of the constituent pigments. This results in spectroscopic differences and a range of dynamical parameters. However, our five-level scheme may be applied to all RCs.

As an example, we consider the Photosystem II reaction center (PSII RC) of green plants. The core of PSII RC consists of six pigment molecules which are closely spaced and coupled by the dipole–dipole interactions forming exciton states. These pigments are held together by a protein matrix consisting of two branches, $D1$ and $D2$. At the center of the PSII RC is a pair of coupled chlorophylls P_{D1} and P_{D2}, which contribute mostly to the lowest energy states and are the primary electron donors. They form two exciton states which are denoted as a_1 and a_2. They are analogous to the special pair of bacteriochlorophylls in the bacterial RC. In PSII RC, these two molecules are also coupled to the accessory chlorophylls Acc_{D1} and Acc_{D2} located in two different branches. Only the donor $D1$ branch takes an active part in the electron transfer process and therefore we consider only the Acc_{D1} accessory molecule in our model. The remaining two pheophytin pigments are coupled to the rest of the molecules. Phe_{D1} is the final electron acceptor in the PSII RC charge-separation process.

Electron transfer in the PSII RC has been thoroughly investigated and several charge-separation pathways were identified. One of the pathways involves the formation of a radical pair $P_{D1}^{+}Acc_{D1}^{-}$ from an excited state which involves P_{D1} and P_{D2}. This is described in our model as a transition between the states a_1, a_2 and the radical pair state α. Then the electron moves further along the multiple sequence of transfer events generating a current between levels α and β, finally returning to the ground state b.

1. Scully MO, Zubairy MS (1997) *Quantum Optics* (Cambridge Univ Press, Cambridge, England).
2. Breuer H-P, Petruccione F (2002) *The Theory of Open Quantum Systems* (Oxford Univ Press, New York).
3. Scully MO, Chapin KR, Dorfman KE, Kim MB, Svidzinsky AA (2011) Quantum heat engine power can be increased by noise-induced coherence. *Proc Natl Acad Sci USA* 108(37):15097–15100.
4. Schulten K (1999) From simplicity to complexity and back. *Simplicity and Complexity in Proteins and Nucleic Acids*, eds Frauenfelder H, Deisenhofer J, Wolynes PJ (Dahlem Univ Press, Berlin, Germany).
5. Agarwal G (1974) *Quantum Statistical Theories of Spontaneous Emission and Their Relation to Other Approaches, Springer Tracts in Modern Physics* (Springer, Berlin), Vol 70.
6. Kozlov VV, Rostovtsev Y, Scully MO (2006) Inducing quantum coherence via decays and incoherent pumping with application to population trapping, lasing without inversion, and quenching of spontaneous emission. *Phys Rev A* 74:063829.

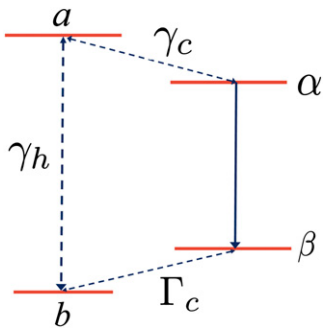

Fig. S1. Generic scheme of a four-level QHE.

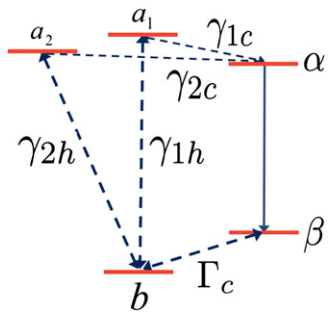

Fig. S2. Generic scheme of a five-level QHE with an upper doublet a_1, a_2 that can exhibit noise-induced coherence.

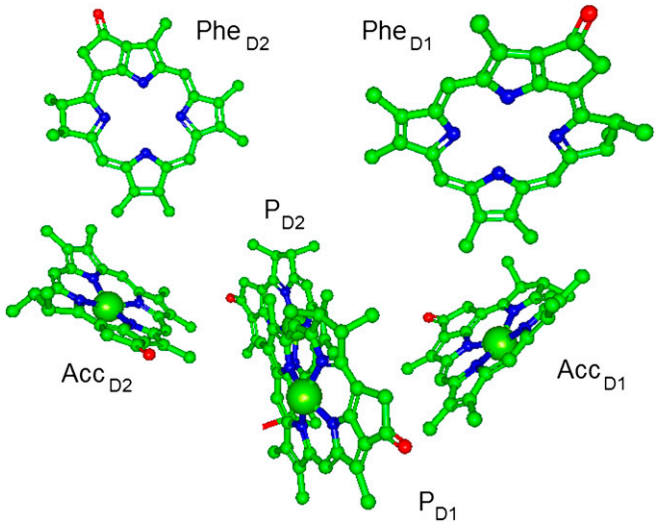

Fig. S3. Structure of the PSII RC [generated using atomic coordinates from the Protein Data Bank, www.rcsb.org (PDB ID code 1IZL)].